16. STRUCTURE FUNCTIONS

Updated July 2009 by B. Foster (University of Oxford), A.D. Martin (University of Durham), and M.G. Vincter (Carleton University).

16.1. Deep inelastic scattering

High-energy lepton-nucleon scattering (deep inelastic scattering) plays a key role in determining the partonic structure of the proton. The process $\ell N \to \ell' X$ is illustrated in Fig. 16.1. The filled circle in this figure represents the internal structure of the proton which can be expressed in terms of structure functions.

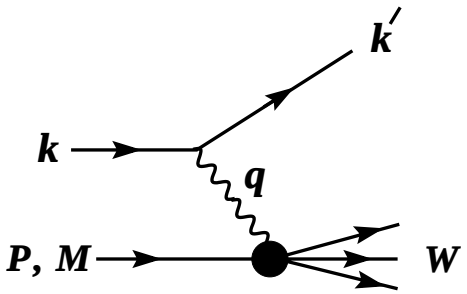

Figure 16.1: Kinematic quantities for the description of deep inelastic scattering. The quantities k and k' are the four-momenta of the incoming and outgoing leptons, P is the four-momentum of a nucleon with mass M, and W is the mass of the recoiling system X. The exchanged particle is a γ, $W^{\pm}$, or Z; it transfers four-momentum $q = k - k'$ to the nucleon.

Invariant quantities:

$\nu = \dfrac{q \cdot P}{M} = E - E'$ is the lepton's energy loss in the nucleon rest frame (in earlier literature sometimes $\nu = q \cdot P$). Here, E and E' are the initial and final lepton energies in the nucleon rest frame.

$Q^2 = -q^2 = 2(EE' - \vec{k} \cdot \vec{k}') - m_\ell^2 - m_{\ell'}^2$ where $m_\ell(m_{\ell'})$ is the initial (final) lepton mass. If $EE' \sin^2(\theta/2) \gg m_\ell^2,\ m_{\ell'}^2$, then

$\approx 4EE' \sin^2(\theta/2)$, where θ is the lepton's scattering angle with respect to the lepton beam direction.

$x = \dfrac{Q^2}{2M\nu}$ where, in the parton model, x is the fraction of the nucleon's momentum carried by the struck quark.

$y = \dfrac{q \cdot P}{k \cdot P} = \dfrac{\nu}{E}$ is the fraction of the lepton's energy lost in the nucleon rest frame.

$W^2 = (P+q)^2 = M^2 + 2M\nu - Q^2$ is the mass squared of the system X recoiling against the scattered lepton.

$s = (k+P)^2 = \dfrac{Q^2}{xy} + M^2 + m_\ell^2$ is the center-of-mass energy squared of the lepton-nucleon system.

The process in Fig. 16.1 is called deep ($Q^2 \gg M^2$) inelastic ($W^2 \gg M^2$) scattering (DIS). In what follows, the masses of the initial and scattered leptons, m_ℓ and $m_{\ell'}$, are neglected.

16.1.1. ***DIS cross sections*** :

$$\frac{d^2\sigma}{dx\,dy} = x\,(s - M^2)\,\frac{d^2\sigma}{dx\,dQ^2} = \frac{2\pi\,M\nu}{E'}\frac{d^2\sigma}{d\Omega_{\rm Nrest}\,dE'}\ . \tag{16.1}$$

In lowest-order perturbation theory, the cross section for the scattering of polarized leptons on polarized nucleons can be expressed in terms of the products of leptonic and hadronic tensors associated with the coupling of the exchanged bosons at the upper and lower vertices in Fig. 16.1 (see Refs. 1–4)

$$\frac{d^2\sigma}{dxdy} \;=\; \frac{2\pi y\alpha^2}{Q^4}\,\sum_j\,\eta_j\,L_j^{\mu\nu}\,W^j_{\mu\nu}\ . \tag{16.2}$$

For neutral-current processes, the summation is over $j = \gamma, Z$ and γZ representing photon and Z exchange and the interference between them, whereas for charged-current interactions there is only W exchange, $j = W$. (For transverse nucleon polarization, there is a dependence on the azimuthal angle of the scattered lepton.) $L_{\mu\nu}$ is the lepton tensor associated with the coupling of the exchange boson to the leptons. For incoming leptons of charge $e = \pm 1$ and helicity $\lambda = \pm 1$,

$$\begin{aligned}
L^\gamma_{\mu\nu} =& 2\left(k_\mu k'_\nu + k'_\mu k_\nu - k\cdot k' g_{\mu\nu} - i\lambda\varepsilon_{\mu\nu\alpha\beta}k^\alpha k'^\beta\right),\\
L^{\gamma Z}_{\mu\nu} =& (g^e_V + e\lambda g^e_A)\,L^\gamma_{\mu\nu}, \qquad L^Z_{\mu\nu} = (g^e_V + e\lambda g^e_A)^2\,L^\gamma_{\mu\nu},\\
L^W_{\mu\nu} =& (1+e\lambda)^2\,L^\gamma_{\mu\nu},
\end{aligned} \tag{16.3}$$

where $g^e_V = -\frac{1}{2} + 2\sin^2\theta_W, \qquad g^e_A = -\frac{1}{2}$.

Although here the helicity formalism is adopted, an alternative approach is to express the tensors in Eq. (16.3) in terms of the polarization of the lepton.

The factors η_j in Eq. (16.2) denote the ratios of the corresponding propagators and couplings to the photon propagator and coupling squared

$$\begin{aligned}
\eta_\gamma \;=\; 1 \quad ;\quad \eta_{\gamma Z} \;=\; & \left(\frac{G_F M_Z^2}{2\sqrt{2}\pi\alpha}\right)\left(\frac{Q^2}{Q^2+M_Z^2}\right);\\
\eta_Z \;=\; \eta^2_{\gamma Z} \quad ;\quad \eta_W \;=\; & \tfrac{1}{2}\left(\frac{G_F M_W^2}{4\pi\alpha}\,\frac{Q^2}{Q^2+M_W^2}\right)^2 .
\end{aligned} \tag{16.4}$$

The hadronic tensor, which describes the interaction of the appropriate electroweak currents with the target nucleon, is given by

$$W_{\mu\nu} \;=\; \frac{1}{4\pi}\int d^4z\,e^{iq\cdot z}\,\left\langle P,S\left|\left[J^\dagger_\mu(z), J_\nu(0)\right]\right|\,P,S\right\rangle, \tag{16.5}$$

where S denotes the nucleon-spin 4-vector, with $S^2 = -M^2$ and $S\cdot P = 0$.

16.2. Structure functions of the proton

The structure functions are defined in terms of the hadronic tensor (see Refs. 1–3)

$$\begin{aligned} W_{\mu\nu} = & \left(-g_{\mu\nu} \; + \; \frac{q_\mu q_\nu}{q^2}\right) \; F_1(x,Q^2) + \frac{\hat{P}_\mu \hat{P}_\nu}{P\cdot q} \; F_2(x,Q^2) \\ & - \; i\varepsilon_{\mu\nu\alpha\beta} \; \frac{q^\alpha P^\beta}{2P\cdot q} \; F_3(x,Q^2) \\ & + \; i\varepsilon_{\mu\nu\alpha\beta} \; \frac{q^\alpha}{P\cdot q} \; \left[S^\beta g_1(x,Q^2) + \left(S^\beta \; - \; \frac{S\cdot q}{P\cdot q} \; P^\beta\right) \; g_2(x,Q^2)\right] \\ & + \; \frac{1}{P\cdot q} \; \left[\tfrac{1}{2}\left(\hat{P}_\mu \hat{S}_\nu \; + \; \hat{S}_\mu \hat{P}_\nu\right) - \frac{S\cdot q}{P\cdot q} \; \hat{P}_\mu \hat{P}_\nu\right] \; g_3(x,Q^2) \\ & + \; \frac{S\cdot q}{P\cdot q} \; \left[\frac{\hat{P}_\mu \hat{P}_\nu}{P\cdot q} \; g_4(x,Q^2) + \left(-g_{\mu\nu} \; + \; \frac{q_\mu q_\nu}{q^2}\right) \; g_5(x,Q^2)\right] \end{aligned} \tag{16.6}$$

where

$$\hat{P}_\mu \; = \; P_\mu \; - \; \frac{P\cdot q}{q^2} \; q_\mu, \qquad \hat{S}_\mu \; = \; S_\mu \; - \; \frac{S\cdot q}{q^2} \; q_\mu \; . \tag{16.7}$$

In Ref. [2], the definition of $W_{\mu\nu}$ with $\mu \leftrightarrow \nu$ is adopted, which changes the sign of the $\varepsilon_{\mu\nu\alpha\beta}$ terms in Eq. (16.6), although the formulae given here below are unchanged. Ref. [1] tabulates the relation between the structure functions defined in Eq. (16.6) and other choices available in the literature.

The cross sections for neutral- and charged-current deep inelastic scattering on unpolarized nucleons can be written in terms of the structure functions in the generic form

$$\begin{aligned} \frac{d^2\sigma^i}{dxdy} \; = \; & \frac{4\pi\alpha^2}{xyQ^2} \; \eta^i \left\{\left(1 \; - \; y \; - \; \frac{x^2y^2M^2}{Q^2}\right) \; F_2^i \right. \\ & \left. + \, y^2 x F_1^i \; \mp \; \left(y \; - \; \frac{y^2}{2}\right) \; xF_3^i\right\}, \end{aligned} \tag{16.8}$$

where i = NC, CC corresponds to neutral-current ($eN \to eX$) or charged-current ($eN \to \nu X$ or $\nu N \to eX$) processes, respectively. For incoming neutrinos, $L^W_{\mu\nu}$ of Eq. (16.3) is still true, but with e, λ corresponding to the outgoing charged lepton. In the last term of Eq. (16.8), the $-$ sign is taken for an incoming e^+ or $\overline{\nu}$ and the $+$ sign for an incoming e^- or ν. The factor $\eta^{\rm NC} = 1$ for unpolarized $e^\pm$ beams, whereas*

$$\eta^{\rm CC} \; = \; (1 \pm \lambda)^2 \eta_W \tag{16.9}$$

with $\pm$ for $\ell^\pm$; and where λ is the helicity of the incoming lepton and η_W is defined in Eq. (16.4); for incoming neutrinos $\eta^{\rm CC} = 4\eta_W$. The CC structure functions, which derive exclusively from W exchange, are

$$F_1^{\rm CC} = F_1^W, \; F_2^{\rm CC} = F_2^W, \; xF_3^{\rm CC} = xF_3^W. \tag{16.10}$$

The NC structure functions $F_2^\gamma, F_2^{\gamma Z}, F_2^Z$ are, for $e^\pm N \to e^\pm X$, given by Ref. [5],

$$F_2^{\rm NC} \;=\; F_2^\gamma \;-\; (g_V^e \pm \lambda g_A^e)\eta_{\gamma Z} F_2^{\gamma Z} \;+\; (g_V^{e\,2} + g_A^{e\,2} \pm 2\lambda g_V^e g_A^e)\,\eta_Z F_2^Z \tag{16.11}$$

and similarly for $F_1^{\rm NC}$, whereas

$$xF_3^{\rm NC} = \; -(g_A^e \pm \lambda g_V^e)\eta_{\gamma Z} x F_3^{\gamma Z} + [2 g_V^e g_A^e \pm \lambda (g_V^{e\,2} + g_A^{e\,2})]\eta_Z x F_3^Z \;. \tag{16.12}$$

The polarized cross-section difference

$$\Delta\sigma \;=\; \sigma(\lambda_n = -1, \lambda_\ell) \;-\; \sigma(\lambda_n = 1, \lambda_\ell) \;, \tag{16.13}$$

where λ_ℓ, λ_n are the helicities (± 1) of the incoming lepton and nucleon, respectively, may be expressed in terms of the five structure functions $g_{1,\ldots 5}(x, Q^2)$ of Eq. (16.6). Thus,

$$\begin{aligned}
\frac{d^2\Delta\sigma^i}{dxdy} \;=\; & \frac{8\pi\alpha^2}{xyQ^2}\,\eta^i \left\{ -\lambda_\ell y \left(2 - y - 2x^2y^2\frac{M^2}{Q^2}\right)\, x g_1^i + \lambda_\ell 4x^3y^2\,\frac{M^2}{Q^2}\, g_2^i \right. \\
& +\; 2x^2 y \frac{M^2}{Q^2}\left(1 - y - x^2y^2\frac{M^2}{Q^2}\right)\, g_3^i \\
& \left. -\; \left(1 + 2x^2y\frac{M^2}{Q^2}\right)\left[\left(1 - y - x^2y^2\frac{M^2}{Q^2}\right)\, g_4^i + xy^2 g_5^i\right]\right\}
\end{aligned} \tag{16.14}$$

with $i =$ NC or CC as before. The Eq. (16.13) corresponds to the difference of antiparallel minus parallel spins of the incoming particles for e^- or ν initiated reactions, but the difference of parallel minus antiparallel for e^+ or $\overline{\nu}$ initiated processes. For longitudinal nucleon polarization, the contributions of g_2 and g_3 are suppressed by powers of M^2/Q^2. These structure functions give an unsuppressed contribution to the cross section for transverse polarization [1], but in this case the cross-section difference vanishes as $M/Q \to 0$.

Because the same tensor structure occurs in the spin-dependent and spin-independent parts of the hadronic tensor of Eq. (16.6) in the $M^2/Q^2 \to 0$ limit, the differential cross-section difference of Eq. (16.14) may be obtained from the differential cross section Eq. (16.8) by replacing

$$F_1 \;\to\; -g_5 \;, \quad F_2 \;\to\; -g_4 \;, \quad F_3 \;\to\; 2g_1 \;, \tag{16.15}$$

and multiplying by two, since the total cross section is the average over the initial-state polarizations. In this limit, Eq. (16.8) and Eq. (16.14) may be written in the form

$$\begin{aligned}
\frac{d^2\sigma^i}{dxdy} &= \frac{2\pi\alpha^2}{xyQ^2}\,\eta^i \left[Y_+ F_2^i \mp Y_- x F_3^i - y^2 F_L^i\right], \\
\frac{d^2\Delta\sigma^i}{dxdy} &= \frac{4\pi\alpha^2}{xyQ^2}\,\eta^i \left[-Y_+ g_4^i \mp Y_- 2x g_1^i + y^2 g_L^i\right],
\end{aligned} \tag{16.16}$$

with $i =$ NC or CC, where $Y_\pm = 1 \pm (1-y)^2$ and

$$F_L^i \;=\; F_2^i \;-\; 2xF_1^i \;, \qquad g_L^i \;=\; g_4^i \;-\; 2xg_5^i \;. \tag{16.17}$$

In the naive quark-parton model, the analogy with the Callan-Gross relations [6] $F_L^i = 0$, are the Dicus relations [7] $g_L^i = 0$. Therefore, there are only two independent polarized structure functions: g_1 (parity conserving) and g_5 (parity violating), in analogy with the unpolarized structure functions F_1 and F_3.

16.2.1. *Structure functions in the quark-parton model* :

In the quark-parton model [8,9], contributions to the structure functions F^i and g^i can be expressed in terms of the quark distribution functions $q(x, Q^2)$ of the proton, where $q = u, \overline{u}, d, \overline{d}$ *etc.*The quantity $q(x, Q^2)dx$ is the number of quarks (or antiquarks) of designated flavor that carry a momentum fraction between x and $x + dx$ of the proton's momentum in a frame in which the proton momentum is large.

For the neutral-current processes $ep \to eX$,

$$\begin{aligned}
\left[F_2^\gamma,\; F_2^{\gamma Z},\; F_2^Z\right] &= x\sum_q \left[e_q^2,\; 2e_q g_V^q,\; {g_V^q}^2 + {g_A^q}^2\right]\;(q+\overline{q})\;,\\
\left[F_3^\gamma,\; F_3^{\gamma Z},\; F_3^Z\right] &= \sum_q \left[0,\; 2e_q g_A^q,\; 2g_V^q g_A^q\right]\;(q-\overline{q})\;,\\
\left[g_1^\gamma,\; g_1^{\gamma Z},\; g_1^Z\right] &= \tfrac{1}{2}\sum_q \left[e_q^2,\; 2e_q g_V^q,\; {g_V^q}^2 + {g_A^q}^2\right]\;(\Delta q+\Delta\overline{q})\;,\\
\left[g_5^\gamma,\; g_5^{\gamma Z},\; g_5^Z\right] &= \sum_q \left[0,\; e_q g_A^q,\; g_V^q g_A^q\right]\;(\Delta q-\Delta\overline{q})\;,
\end{aligned} \tag{16.18}$$

where $g_V^q = \pm\frac{1}{2} - 2e_q \sin^2\theta_W$ and $g_A^q = \pm\frac{1}{2}$, with $\pm$ according to whether q is a $u-$ or $d-$type quark respectively. The quantity Δq is the difference $q\uparrow - q\downarrow$ of the distributions with the quark spin parallel and antiparallel to the proton spin.

For the charged-current processes $e^- p \to \nu X$ and $\overline{\nu} p \to e^+ X$, the structure functions are:

$$\begin{aligned}
F_2^{W^-} &= 2x(u + \overline{d} + \overline{s} + c\ldots)\;,\\
F_3^{W^-} &= 2(u - \overline{d} - \overline{s} + c\ldots)\;,\\
g_1^{W^-} &= (\Delta u + \Delta\overline{d} + \Delta\overline{s} + \Delta c\ldots)\;,\\
g_5^{W^-} &= (-\Delta u + \Delta\overline{d} + \Delta\overline{s} - \Delta c\ldots)\;,
\end{aligned} \tag{16.19}$$

where only the active flavors are to be kept and where CKM mixing has been neglected. For $e^+ p \to \overline{\nu} X$ and $\nu p \to e^- X$, the structure functions F^{W^+}, g^{W^+} are obtained by the flavor interchanges $d \leftrightarrow u, s \leftrightarrow c$ in the expressions for F^{W^-}, g^{W^-}. The structure functions for scattering on a neutron are obtained from those of the proton by the

interchange $u \leftrightarrow d$. For both the neutral- and charged-current processes, the quark-parton model predicts $2xF_1^i = F_2^i$ and $g_4^i = 2xg_5^i$.

Neglecting masses, the structure functions g_2 and g_3 contribute only to scattering from transversely polarized nucleons (for which $S \cdot q = 0$), and have no simple interpretation in terms of the quark-parton model. They arise from off-diagonal matrix elements $\langle P, \lambda' | [J_\mu^\dagger(z), J_\nu(0)] | P, \lambda \rangle$, where the proton helicities satisfy $\lambda' \neq \lambda$. In fact, the leading-twist contributions to both g_2 and g_3 are both twist-2 and twist-3, which contribute at the same order of Q^2. The Wandzura-Wilczek relation [10] expresses the twist-2 part of g_2 in terms of g_1 as

$$g_2^i(x) \;=\; -g_1^i(x) \;+\; \int_x^1 \frac{dy}{y}\, g_1^i(y)\;. \tag{16.20}$$

However, the twist-3 component of g_2 is unknown. Similarly, there is a relation expressing the twist-2 part of g_3 in terms of g_4. A complete set of relations, including M^2/Q^2 effects, can be found in Ref. [11].

16.2.2. *Structure functions and QCD* :

One of the most striking predictions of the quark-parton model is that the structure functions F_i, g_i *scale*, *i.e.*, $F_i(x, Q^2) \to F_i(x)$ in the Bjorken limit that Q^2 and $\nu \to \infty$ with x fixed [12]. This property is related to the assumption that the transverse momentum of the partons in the infinite-momentum frame of the proton is small. In QCD, however, the radiation of hard gluons from the quarks violates this assumption, leading to logarithmic scaling violations, which are particularly large at small x, see Fig. 16.2. The radiation of gluons produces the evolution of the structure functions. As Q^2 increases, more and more gluons are radiated, which in turn split into $q\overline{q}$ pairs. This process leads both to the softening of the initial quark momentum distributions and to the growth of the gluon density and the $q\overline{q}$ sea as x decreases.

In QCD, the above process is described in terms of scale-dependent parton distributions $f_a(x, \mu^2)$, where $a = g$ or q and, typically, μ is the scale of the probe Q. For $Q^2 \gg M^2$, the structure functions are of the form

$$F_i = \sum_a C_i^a \otimes f_a, \tag{16.21}$$

where $\otimes$ denotes the convolution integral

$$C \;\otimes\; f \;=\; \int_x^1 \frac{dy}{y}\, C(y)\, f\left(\frac{x}{y}\right)\;, \tag{16.22}$$

and where the coefficient functions C_i^a are given as a power series in α_s. The parton distribution f_a corresponds, at a given x, to the density of parton a in the proton integrated over transverse momentum k_t up to μ. Its evolution in μ is described in QCD by a DGLAP equation (see Refs. 14–17) which has the schematic form

$$\frac{\partial f_a}{\partial \ln \mu^2} \sim \frac{\alpha_s(\mu^2)}{2\pi} \sum_b \left(P_{ab} \otimes f_b\right)\;, \tag{16.23}$$

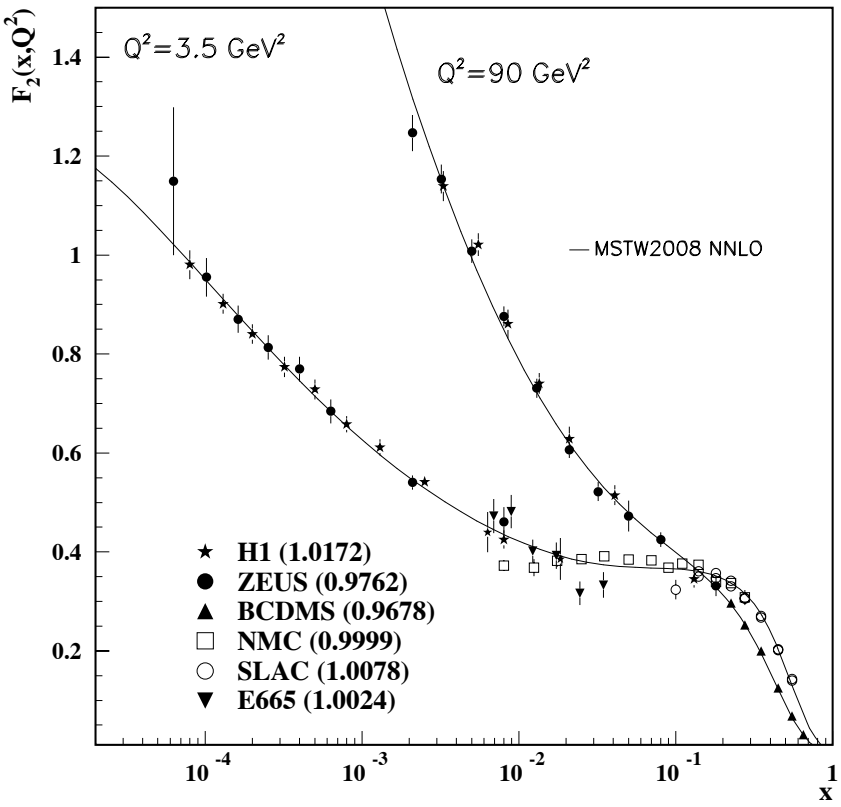

Figure 16.2: The proton structure function F_2^p given at two Q^2 values (3.5 GeV^2 and 90 GeV^2), which exhibit scaling at the 'pivot' point $x \sim 0.14$. See the captions in Fig. 16.7 and Fig. 16.10 for the references of the data. The various data sets have been renormalised by the factors shown in brackets in the key to the plot, which were determined in the NNLO MSTW2008 global analysis, see Table 3 of [13].

where the P_{ab}, which describe the parton splitting $b \to a$, are also given as a power series in α_s. Although perturbative QCD can predict, via Eq. (16.23), the evolution of the parton distribution functions from a particular scale, μ_0, these DGLAP equations cannot predict them *a priori* at any particular μ_0. Thus they must be measured at a starting point μ_0 before the predictions of QCD can be compared to the data at other scales, μ. In general, all observables involving a hard hadronic interaction (such as structure functions) can be expressed as a convolution of calculable, process-dependent coefficient functions and these universal parton distributions, e.g. Eq. (16.21).

It is often convenient to write the evolution equations in terms of the gluon, non-singlet (q^{NS}) and singlet (q^S) quark distributions, such that

$$q^{NS} \;=\; q_i - \overline{q}_i \quad (\text{or } \; q_i - q_j), \qquad q^S \;=\; \sum_i (q_i + \overline{q}_i) \; . \tag{16.24}$$

The non-singlet distributions have non-zero values of flavor quantum numbers, such as isospin and baryon number. The DGLAP evolution equations then take the form

$$\frac{\partial q^{NS}}{\partial \ln \mu^2} = \frac{\alpha_s(\mu^2)}{2\pi}\, P_{qq} \otimes q^{NS} \ ,$$

$$\frac{\partial}{\partial \ln \mu^2} \begin{pmatrix} q^S \\ g \end{pmatrix} = \frac{\alpha_s(\mu^2)}{2\pi} \begin{pmatrix} P_{qq} & 2n_f\, P_{qg} \\ P_{gq} & P_{gg} \end{pmatrix} \otimes \begin{pmatrix} q^S \\ g \end{pmatrix} \ , \tag{16.25}$$

where P are splitting functions that describe the probability of a given parton splitting into two others, and n_f is the number of (active) quark flavors. The leading-order Altarelli-Parisi [16] splitting functions are

$$P_{qq} = \tfrac{4}{3}\left[\frac{1+x^2}{(1-x)}\right]_+ = \tfrac{4}{3}\left[\frac{1+x^2}{(1-x)_+}\right] + 2\delta(1-x) \ , \tag{16.26}$$

$$P_{qg} = \tfrac{1}{2}\left[x^2 + (1-x)^2\right] \ , \tag{16.27}$$

$$P_{gq} = \tfrac{4}{3}\left[\frac{1+(1-x)^2}{x}\right] \ , \tag{16.28}$$

$$P_{gg} = 6\left[\frac{1-x}{x} + x(1-x) + \frac{x}{(1-x)_+}\right] + \left[\frac{11}{2} - \frac{n_f}{3}\right]\delta(1-x), \tag{16.29}$$

where the notation $[F(x)]_+$ defines a distribution such that for any sufficiently regular test function, $f(x)$,

$$\int_0^1 dx f(x)[F(x)]_+ = \int_0^1 dx\ (f(x) - f(1))F(x) \ . \tag{16.30}$$

In general, the splitting functions can be expressed as a power series in α_s. The series contains both terms proportional to $\ln \mu^2$ and to $\ln\ 1/x$. The leading-order DGLAP evolution sums up the $(\alpha_s \ln \mu^2)^n$ contributions, while at next-to-leading order (NLO) the sum over the $\alpha_s(\alpha_s \ln \mu^2)^{n-1}$ terms is included [18,19]. In fact, the NNLO contributions to the splitting functions and the DIS coefficient functions are now also all known [20–22].

In the kinematic region of very small x, it is essential to sum leading terms in $\ln\ 1/x$, independent of the value of $\ln \mu^2$. At leading order, LLx, this is done by the BFKL equation for the unintegrated distributions (see Refs. [23,24]). The leading-order $(\alpha_s \ln(1/x))^n$ terms result in a power-like growth, $x^{-\omega}$ with $\omega = (12\alpha_s \ln 2)/\pi$, at asymptotic values of $\ln\ 1/x$. More recently, the next-to-leading $\ln\ 1/x$ (NLLx) contributions have become available [25,26]. They are so large (and negative) that the result appears to be perturbatively unstable. Methods, based on a combination of collinear and small x resummations, have been developed which reorganize the perturbative series into a more stable hierarchy [27–30]. There are indications that small

x resummations become necessary for real precision for $x \lesssim 10^{-3}$ at low scales. On the other hand, there is no convincing indication that, for $Q^2 \gtrsim 2$ GeV^2, we have entered the 'non-linear' regime where the gluon density is so high that gluon-gluon recombination effects become significant.

The precision of the contemporary experimental data demands that at least NLO, and preferably NNLO, DGLAP evolution be used in comparisons between QCD theory and experiment. Beyond the leading order, it is necessary to specify, and to use consistently, both a renormalization and a factorization scheme. The renormalization scheme used is almost universally the modified minimal subtraction ($\overline{\rm MS}$) scheme [31,32]. There are two popular choices for factorization scheme, in which the form of the correction for each structure function is different. The most-used factorization scheme is again $\overline{\rm MS}$ [33]. However, sometimes the DIS [34] scheme is adopted, in which there are no higher-order corrections to the F_2 structure function. The two schemes differ in how the non-divergent pieces are assimilated in the parton distribution functions.

The u, d, and s quarks are taken to be massless, and the effects of the c and b-quark masses have been studied up to NNLO, for example, in [35–41]. An approach using a variable flavor number is now generally adopted, in which evolution with $n_f = 3$ is matched to that with $n_f = 4$ at the charm threshold, with an analogous matching at the bottom threshold.

The discussion above relates to the Q^2 behavior of leading-twist (twist-2) contributions to the structure functions. Higher-twist terms, which involve their own non-perturbative input, exist. These die off as powers of Q; specifically twist-n terms are damped by $1/Q^{n-2}$. The higher-twist terms appear to be numerically unimportant for Q^2 above a few GeV^2, except for x close to 1.

16.3. Determination of parton distributions

The parton distribution functions (PDFs) can be determined from data for deep inelastic lepton-nucleon scattering and for related hard-scattering processes initiated by nucleons. Table 16.1 highlights some processes and their primary sensitivity to PDFs.

The kinematic ranges of fixed-target and collider experiments are complementary (as is shown in Fig. 16.3), which enables the determination of PDFs over a wide range in x and Q^2. Recent determinations of the unpolarized PDF's from NLO global analyses are given in Ref. [13,42], see also Ref. [43] for progress towards a neural network global analysis. NNLO global analyses are given in Ref. [13,44]. The results of one analysis are shown in Fig. 16.4 at scales $\mu^2 = 10$ and 10^4 GeV^2.

Spin-dependent (or polarized) PDFs have been obtained through NLO global analyses which include measurements of the g_1 structure function in inclusive polarized DIS, 'flavour-tagged' semi-inclusive DIS data, and results from polarized pp scattering at RHIC. Recent NLO analyses are given in Refs. [45–47]. Improved parton-to-hadron fragmentation functions, needed to describe the semi-inclusive DIS data, can be found in [48–50]. Fig. 16.5 shows several global analyses at a scale of 2.5 GeV^2 along with the data from semi-inclusive DIS.

Table 16.1: The main processes included in the current global PDF analyses, ordered in three groups: fixed-target experiments, HERA and the Tevatron. For each process we give an indication of their dominant partonic subprocesses, the primary partons which are probed and the approximate range of x constrained by the data. The Table is taken from [13].

Process	Subprocess	Partons	x range
$\ell^\pm \{p,n\} \to \ell^\pm X$	$\gamma^* q \to q$	$q, \bar{q}, g$	$x \gtrsim 0.01$
$\ell^\pm n/p \to \ell^\pm X$	$\gamma^* d/u \to d/u$	d/u	$x \gtrsim 0.01$
$pp \to \mu^+\mu^- X$	$u\bar{u}, d\bar{d} \to \gamma^*$	$\bar{q}$	$0.015 \lesssim x \lesssim 0.35$
$pn/pp \to \mu^+\mu^- X$	$(u\bar{d})/(u\bar{u}) \to \gamma^*$	$\bar{d}/\bar{u}$	$0.015 \lesssim x \lesssim 0.35$
$\nu(\bar{\nu})\, N \to \mu^-(\mu^+)\, X$	$W^* q \to q'$	$q, \bar{q}$	$0.01 \lesssim x \lesssim 0.5$
$\nu\, N \to \mu^-\mu^+ X$	$W^* s \to c$	s	$0.01 \lesssim x \lesssim 0.2$
$\bar{\nu}\, N \to \mu^+\mu^- X$	$W^* \bar{s} \to \bar{c}$	$\bar{s}$	$0.01 \lesssim x \lesssim 0.2$
$e^\pm p \to e^\pm X$	$\gamma^* q \to q$	$g, q, \bar{q}$	$0.0001 \lesssim x \lesssim 0.1$
$e^+ p \to \bar{\nu} X$	$W^+ \{d,s\} \to \{u,c\}$	d, s	$x \gtrsim 0.01$
$e^\pm p \to e^\pm c\bar{c} X$	$\gamma^* c \to c$, $\gamma^* g \to c\bar{c}$	c, g	$0.0001 \lesssim x \lesssim 0.01$
$e^\pm p \to$ jet$+X$	$\gamma^* g \to q\bar{q}$	g	$0.01 \lesssim x \lesssim 0.1$
$p\bar{p} \to$ jet$+X$	$gg, qg, qq \to 2j$	g, q	$0.01 \lesssim x \lesssim 0.5$
$p\bar{p} \to (W^\pm \to \ell^\pm\nu)\, X$	$ud \to W, \bar{u}\bar{d} \to W$	$u, d, \bar{u}, \bar{d}$	$x \gtrsim 0.05$
$p\bar{p} \to (Z \to \ell^+\ell^-)\, X$	$uu, dd \to Z$	d	$x \gtrsim 0.05$

Comprehensive sets of PDFs are available as program-callable functions from the HepData website [55], which includes comparison graphics of PDFs, and from the LHAPDF library [56], which can be linked directly into a users programme to provide access to recent PDFs in a standard format.

16.4. DIS determinations of α_s

Table 16.2 shows the values of $\alpha_s(M_Z^2)$ found in recent fits to DIS and related data in which the coupling is left as a free parameter. There have been several other studies of α_s using subsets of inclusive DIS data, and also from measurements of spin-dependent structure functions, see the Quantum Chromodynamics section of this *Review*.

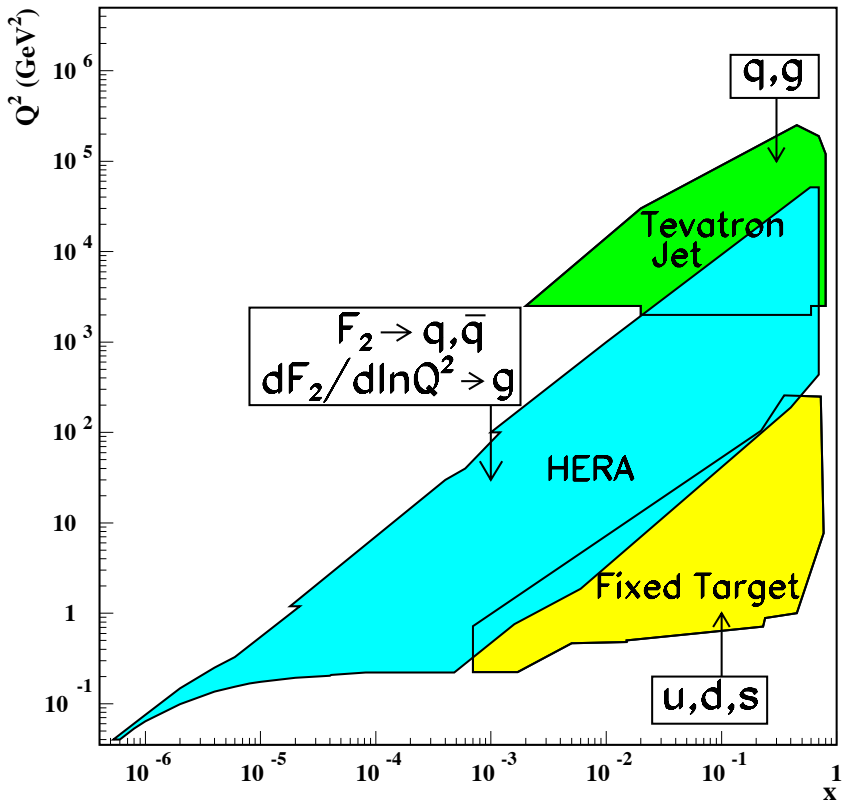

Figure 16.3: Kinematic domains in x and Q^2 probed by fixed-target and collider experiments, shown together with the parton distributions that are most strongly constrained by the indicated regions.

16.5. The hadronic structure of the photon

Besides the *direct* interactions of the photon, it is possible for it to fluctuate into a hadronic state via the process $\gamma \to q\overline{q}$. While in this state, the partonic content of the photon may be *resolved*, for example, through the process $e^+e^- \to e^+e^-\gamma^*\gamma \to e^+e^-X$, where the virtual photon emitted by the DIS lepton probes the hadronic structure of the quasi-real photon emitted by the other lepton. The perturbative LO contributions, $\gamma \to q\overline{q}$ followed by $\gamma^* q \to q$, are subject to QCD corrections due to the coupling of quarks to gluons.

Often the equivalent-photon approximation is used to express the differential cross section for deep inelastic electron–photon scattering in terms of the structure functions of the transverse quasi-real photon times a flux factor N_γ^T (for these incoming quasi-real photons of transverse polarization)

$$\frac{d^2\sigma}{dxdQ^2} = N_\gamma^T \frac{2\pi\alpha^2}{xQ^4}\left[\left(1+(1-y)^2\right)F_2^\gamma(x,Q^2) - y^2 F_L^\gamma(x,Q^2)\right],$$

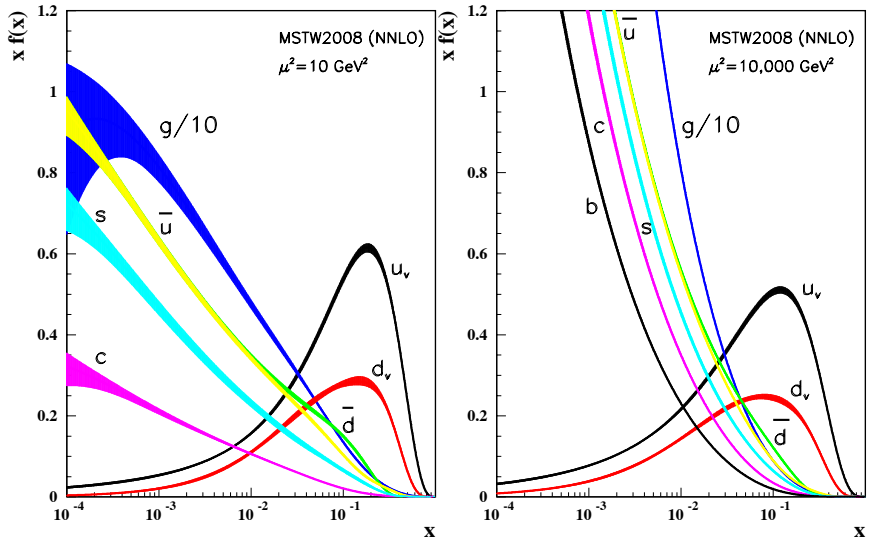

Figure 16.4: Distributions of x times the unpolarized parton distributions $f(x)$ (where $f = u_v, d_v, \overline{u}, \overline{d}, s, c, b, g$) and their associated uncertainties using the NNLO MSTW2008 parameterization [13] at a scale $\mu^2 = 10$ GeV^2 and $\mu^2 = 10,000$ GeV^2.

where we have used $F_2^\gamma = 2xF_T^\gamma + F_L^\gamma$, not to be confused with F_2^γ of Sec. 16.2. Complete formulae are given, for example, in the comprehensive review of Ref. [62].

The hadronic photon structure function, F_2^γ, evolves with increasing Q^2 from the 'hadron-like' behavior, calculable via the vector-meson-dominance model, to the dominating 'point-like' behaviour, calculable in perturbative QCD. Due to the point-like coupling, the logarithmic evolution of F_2^γ with Q^2 has a *positive* slope for all values of x, see Fig. 16.14. The 'loss' of quarks at large x due to gluon radiation is over-compensated by the 'creation' of quarks via the point-like $\gamma \to q\bar{q}$ coupling. The logarithmic evolution was first predicted in the quark–parton model ($\gamma^*\gamma \to q\bar{q}$) [63,64], and then in QCD in the limit of large Q^2 [65]. The evolution is now known to NLO [66–68]. NLO data analyses to determine the parton densities of the photon can be found in [69–71].

16.6. Diffractive DIS (DDIS)

Some 10% of DIS events are diffractive, $\gamma^* p \to X + p$, in which the slightly deflected proton and the cluster X of outgoing hadrons are well-separated in rapidity. Besides x and Q^2, two extra variables are needed to describe a DDIS event: the fraction $x_{I\!P}$ of the proton's momentum transferred across the rapidity gap and t, the square of the 4-momentum transfer of the proton. The DDIS data [72–76] are usually analyzed using two levels of factorization. First, the diffractive structure function $F_2^{\rm D}$ satisfies *collinear factorization*, and can be expressed as the convolution [77]

$$F_2^{\rm D} = \sum_{a=q,g} C_2^a \otimes f_{a/p}^{\rm D}, \tag{16.31}$$

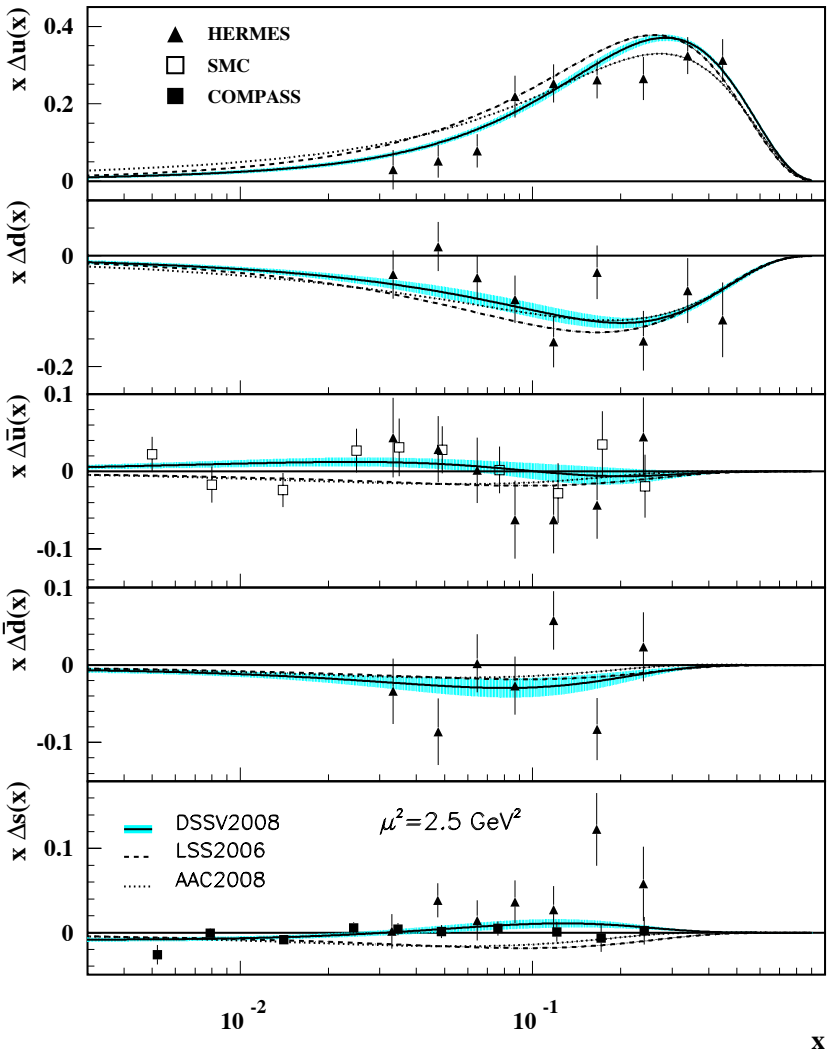

Figure 16.5: Distributions of x times the polarized parton distributions $\Delta q(x)$ (where $q = u, d, \overline{u}, \overline{d}, s$) using the LSS2006 [45], AAC2008 [46], and DSSV2008 [47] parameterizations at a scale $\mu^2 = 2.5$ GeV^2, showing the error corridor of the latter set (corresponding to a one-unit increase in χ^2). Points represent data from semi-inclusive positron (HERMES [51,52]) and muon (SMC [53] and COMPASS [54]) deep inelastic scattering given at $Q^2 = 2.5$ GeV^2. SMC results are extracted under the assumption that $\Delta\overline{u}(x) = \Delta\overline{d}(x)$.

with the same coefficient functions as in DIS (see Eq. (16.21)), and where the diffractive parton distributions $f^{\rm D}_{a/p}$ $(a = q, g)$ satisfy DGLAP evolution. Second, *Regge factorization* is assumed [78],

$$f^{\rm D}_{a/p}(x_{I\!P}, t, z, \mu^2) = f_{I\!P/p}(x_{I\!P}, t)\, f_{a/I\!P}(z, \mu^2), \tag{16.32}$$

where $f_{a/I\!P}$ are the parton densities of the Pomeron, which itself is treated like a hadron, and $z \in [x/x_{I\!P}, 1]$ is the fraction of the Pomeron's momentum carried by the

Table 16.2: The values of $\alpha_s(M_Z^2)$ found in NLO and NNLO fits to DIS and related data. CTEQ [57] and MSTW [58] are global fits. H1 [59] fit only a subset of the F_2^{ep} data, while Alekhin [61] also includes F_2^{ed} and ZEUS [60] in addition include their charged current and jet data. At NNLO, Alekhin *et al.* [44] include Drell-Yan data in their fit. The experimental errors quoted correspond to 68% C.L. See [58] for an extended comparative discussion.

	$\alpha_s(M_Z^2) \pm$ expt $\pm$ theory $\pm$ model	
NLO		
CTEQ	0.1170 ± 0.0047	
MSTW08	$0.1202 \quad ^{+0.0012}_{-0.0015} \pm 0.003$	
ZEUS	0.1183 ± 0.0028	± 0.0008
H1	$0.115 \quad \pm 0.0017 \pm 0.005$	$^{+0.0009}_{-0.0005}$
Alekhin	$0.1171 \pm 0.0015 \pm 0.0033$	
NNLO		
MSTW08	$0.1171 \pm 0.0014 \quad \pm 0.003$	
Alekhin	0.1128 ± 0.0015	

parton entering the hard subprocess. The Pomeron flux factor $f_{I\!P/p}(x_{I\!P}, t)$ is taken from Regge phenomenology. There are also secondary Reggeon contributions to Eq. (16.32). A sample of the t-integrated diffractive parton densities, obtained in this way, is shown in Fig. 16.6 as Fit A.

Although collinear factorization holds as $\mu^2 \to \infty$, there are non-negligible corrections for finite μ^2 and small $x_{I\!P}$. Besides the *resolved* interactions of the Pomeron, the perturbative QCD Pomeron may also interact *directly* with the hard subprocess, giving rise to an inhomogeneous evolution equation for the diffractive parton densities analogous to the photon case. The results of the MRW analysis [79], which includes these contributions, are also shown in Fig. 16.6. Unlike the inclusive case, the diffractive parton densities cannot be directly used to calculate diffractive hadron-hadron cross sections, since account must first be taken of "soft" rescattering effects.

* The value of $\eta^{\rm CC}$ deduced from Ref. [1] is found to be a factor of two too small; $\eta^{\rm CC}$ of Eq. (16.9) agrees with Refs. [2,3].

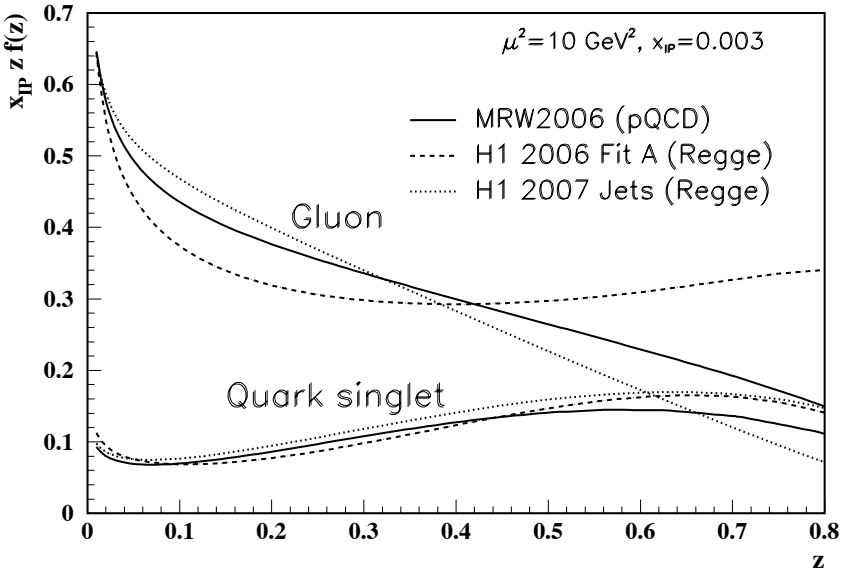

Figure 16.6: Diffractive parton distributions, $x_{I\!P}\, z f^{\rm D}_{a/p}$, obtained from fitting to the H1 data with $Q^2 > 8.5$ GeV^2 assuming Regge factorization [75], and using a more perturbative QCD approach [79]. Only the Pomeron contributions are shown and not the secondary Reggeon contributions which are negligible at the value of $x_{I\!P} = 0.003$ chosen here. Diffractive DIS dijet data [80,81,82] favour a smaller gluon at high z than that in H1 Fit A, more like MRW, as shown by the H1 Jets curve [81].

References:

1. J. Blümlein and N. Kochelev, Nucl. Phys. **B498**, 285 (1997).
2. S. Forte *et al.*, Nucl. Phys. **B602**, 585 (2001).
3. M. Anselmino *et al.*, Z. Phys. **C64**, 267 (1994).
4. M. Anselmino *et al.*, Phys. Rep. **261**, 1 (1995).
5. M. Klein and T. Riemann, Z. Phys. **C24**, 151 (1984).
6. C.G. Callan and D.J. Gross, Phys. Rev. Lett. **22**, 156 (1969).
7. D.A. Dicus, Phys. Rev. **D5**, 1367 (1972).
8. J.D. Bjorken and E.A. Paschos, Phys. Rev. **185**, 1975 (1969).
9. R.P. Feynman, Photon Hadron Interactions (Benjamin, New York, 1972).
10. S. Wandzura and F. Wilczek, Phys. Rev. **B72**, 195 (1977).
11. J. Blümlein and A. Tkabladze, Nucl. Phys. **B553**, 427 (1999).
12. J.D. Bjorken, Phys. Rev. **179**, 1547 (1969).
13. MSTW, A.D. Martin *et al.*, Eur. Phys. J. **C63**, 189 (2009).
14. V.N. Gribov and L.N. Lipatov, Sov. J. Nucl. Phys. **15**, 438 (1972).
15. L.N. Lipatov, Sov. J. Nucl. Phys. **20**, 95 (1975).
16. G. Altarelli and G. Parisi, Nucl. Phys. **B126**, 298 (1977).
17. Yu.L. Dokshitzer, Sov. Phys. JETP **46**, 641 (1977).

18. G. Curci *et al.*, Nucl. Phys. **B175**, 27 (1980); W. Furmanski, and R. Petronzio, Phys. Lett. **B97**, 437 (1980).
19. R.K. Ellis *et al.*, QCD and Collider Physics (Cambridge UP, 1996).
20. E.B. Zijlstra and W.L. van Neerven, Phys. Lett. **B272**, 127 (1991); Phys. Lett. **B273**, 476 (1991); Phys. Lett. **B297**, 377 (1992); Nucl. Phys. **B383**, 525 (1992).
21. S. Moch and J.A.M. Vermaseren, Nucl. Phys. **B573**, 853 (2000).
22. S. Moch *et al.*, Nucl. Phys. **B688**, 101 (2004); Nucl. Phys. **B691**, 129 (2004); Phys. Lett. **B606**, 123 (2005); Nucl. Phys. **B724**, 3 (2005).
23. E.A. Kuraev *et al.*, Phys. Lett. **B60**, 50 (1975); Sov. Phys. JETP **44**, 443 (1976); Sov. Phys. JETP **45**, 199 (1977).
24. Ya.Ya. Balitsky and L.N. Lipatov, Sov. J. Nucl. Phys. **28**, 822 (1978).
25. V.S. Fadin, and L.N. Lipatov, Phys. Lett. **B429**, 127 (1998).
26. G. Camici and M. Ciafaloni, Phys. Lett. **B412**, 396 (1997), erratum-Phys. Lett. **B147**, 390 (1997); Phys. Lett. **B430**, 349 (1998).
27. M. Ciafaloni *et al.*, Phys. Rev. **D60**, 114036 (1999); JHEP **0007** 054 (2000).
28. M. Ciafaloni *et al.*, Phys. Lett. **B576**, 143 (2003); Phys. Rev. **D68**, 114003 (2003).
29. G. Altarelli *et al.*, Nucl. Phys. **B742**, 1 (2006); Nucl. Phys. **B799**, 199 (2008).
30. C.D. White and R.S. Thorne, Phys. Rev. **D75**, 034005 (2007).
31. G. 't Hooft and M. Veltman, Nucl. Phys. **B44**, 189 (1972).
32. G. 't Hooft, Nucl. Phys. **B61**, 455 (1973).
33. W.A. Bardeen *et al.*, Phys. Rev. **D18**, 3998 (1978).
34. G. Altarelli *et al.*, Nucl. Phys. **B143**, 521 (1978) and erratum: Nucl. Phys. **B146**, 544 (1978).
35. M.A.G. Aivazis *et al.*, Phys. Rev. **D50**, 3102 (1994).
36. J.C. Collins, Phys. Rev. **D58**, 094002 (1998).
37. A. Chuvakin *et al.*, Phys. Rev. **D61**, 096004 (2000).
38. R.S. Thorne and R.G. Roberts, Eur. Phys. J. **C19**, 339 (2001).
39. S. Kretzer *et al.*, Phys. Rev. **D69**, 114005 (2004).
40. R.S. Thorne, Phys. Rev. **D73**, 054019 (2006).
41. R.S. Thorne and W.-K. Tung, Proc. 4th HERA-LHC Workshop, arXiv:0809.0714.
42. CTEQ: P.M. Nadolsky *et al.*, Phys. Rev. **D78**, 013004 (2008).
43. NNPDF: R.D. Ball *et al.*, Nucl. Phys. **B809**, 1 (2009), erratum Nucl. Phys. **B816**, 293 (2009); Nucl. Phys. **B823**, 195 (2009).
44. S. Alekhin *et al.*, Phys. Rev. **D74**, 054033 (2006).
45. E. Leader *et al.*, Phys. Rev. **D75**, 0704027 (2007).
46. M. Hirai *et al.*, Nucl. Phys. **B813**, 106 (2009).
47. D. de Florian *et al.*, Phys. Rev. Lett. **101**, 072001 (2008); Phys. Rev. **D80**, 034030 (2009).
48. M. Hirai *et al.*, Phys. Rev. **D75**, 094009 (2007).
49. D. de Florian *et al.*, Phys. Rev. **D75**, 114010 (2007);Phys. Rev. **D76**, 074033 (2007).
50. S. Albino *et al.*, Nucl. Phys. **B803**, 42 (2008).
51. HERMES, A. Airpetian *et al.*, Phys. Rev. Lett. **92**, 012005 (2004); A. Airpetian *et al.*, Phys. Rev. **D71**, 012003 (2005).
52. HERMES, A. Airpetian *et al.*, Phys. Lett. **B666**, 446 (2008).

53. SMC, B. Adeva *et al.*, Phys. Lett. **B420**, 180 (1998).
54. COMPASS, M. Alekseev *et al.*, Phys. Lett. **B680**, 217 (2009).
55. `http://durpdg.dur.ac.uk/hepdata/pdf`.
56. `http://projects.hepforge.org/lhapdf`, see hep-ph/0508110.
57. J. Pumplin *et al.*, JHEP **0602**, 032 (2006).
58. MSTW, A.D. Martin *et al.*, Eur. Phys. J. **C64**, 653 (2009).
59. H1, C. Adloff *et al.*, Eur. Phys. J. **C21**, 33 (2001).
60. ZEUS, S. Chekanov *et al.*, Eur. Phys. J. **C42**, 1 (2005).
61. S. Alekhin, JHEP **0302**, 015 (2003).
62. R. Nisius, Phys. Reports **332**, 165 (2000).
63. T.F. Walsh and P.M. Zerwas, Phys. Lett. **B44**, 195 (1973).
64. R.L. Kingsley, Nucl. Phys. **B60**, 45 (1973).
65. E. Witten, Nucl. Phys. **B120**, 189 (1977).
66. W.A. Bardeen and A.J. Buras, Phys. Rev. **D20**, 166 (1979), erratum Phys. Rev. **D21**, 2041 (1980).
67. M. Fontannaz and E. Pilon, Phys. Rev. **D45**, 382 (1992), erratum Phys. Rev. **D46**, 484 (1992).
68. M. Glück *et al.*, Phys. Rev. **D45**, 3986 (1992).
69. F. Cornet *et al.*, Phys. Rev. **D70**, 093004 (2004).
70. P. Aurenche, *et al.*, Eur. Phys. J. **C44**, 395 (2005).
71. W. Slominski *et al.*, Eur. Phys. J. **C45**, 633 (2006).
72. ZEUS, S. Chekanov *et al.*, Eur. Phys. J. **C38**, 43 (2004).
73. ZEUS, S. Chekanov *et al.*, Nucl. Phys. **B713**, 3 (2005).
74. H1, A. Aktas *et al.*, Eur. Phys. J. **C48**, 749 (2006).
75. H1, A. Aktas *et al.*, Eur. Phys. J. **C48**, 715 (2006).
76. ZEUS, S. Chekanov *et al.*, Nucl. Phys. **B816**, 1 (2009).
77. J. C. Collins, Phys. Rev. **D57**, 3051 (1998); Erratum Phys. Rev. **D61**, 019902 (2000).
78. G. Ingelman and P. E. Schlein, Phys. Lett. **B152**, 256 (1985).
79. A. D. Martin, M. G. Ryskin and G. Watt, Phys. Lett. **B644**, 131 (2007).
80. H1, A. Aktas *et al.*, Eur. Phys. J. **C51**, 549 (2007).
81. H1, A. Aktas *et al.*, JHEP **0710**, 042 (2007).
82. ZEUS, S. Chekanov *et al.*, Eur. Phys. J. **C52**, 813 (2007).